Recent results from Belle

Peter Križan (for the Belle Collaboration)
University of Ljubljana and J. Stefan Institute,
Jadranska 19, SI-1000 Ljubljana, Slovenia

Abstract

The paper reviews recent results from the Belle experiment. We first briefly describe the experimental apparatus, and its performance, and then proceed to discuss recent results, an update of the measurement of the CP violation parameter $\sin 2\phi_1$, a report on the measurement of CP violation in B^0 decays to $\pi^+\pi^-$, $\eta' K_S$, ϕK_S, $K^+K^-K_S$ and $J/\psi\pi^0$ final states, and finally present the measurement of inclusive $b \to s\ell^+\ell^-$ decays.

1 Introduction

The violation of symmetry with respect to a combined C and P transformation is a fundamental quantity, as it distinguishes matter from anti-matter. It is therefore related to the observed striking difference in the abundance of matter and anti-matter in the universe as we see it today.

The history of CP violation measurements started in 1964, when the effect was first observed in K^0 decays. In the three decades to follow, it was extensively studied in the kaon system. The discovery of a large $B^0\bar{B}^0$ mixing rate with the ARGUS spectrometer in 1987 [1] indicated that the CP violating effects could be large in B decays [2]. In subsequent years several projects were proposed to study these effects, and some experiments eventually attempted to measure CP violation in the $B^0\bar{B}^0$ system. The effect was finally observed in 2001 by the two dedicated spectrometers Belle and BaBar at asymmetric e^+e^- colliders - B factories [3, 4].

In the Standard Model (SM), CP violation is accommodated as an irreducible phase in the CKM weak interaction mixing matrix V [5],

$$\begin{pmatrix} V_{ud} & V_{us} & V_{ub} \\ V_{cd} & V_{cs} & V_{cb} \\ V_{td} & V_{ts} & V_{tb} \end{pmatrix} = \begin{pmatrix} 1-\frac{\lambda^2}{2} & \lambda & A\lambda^3(\varrho - i\eta) \\ -\lambda & 1-\frac{\lambda^2}{2} & A\lambda^2 \\ A\lambda^3(1-\varrho - i\eta) & -A\lambda^2 & 1 \end{pmatrix}.$$

Unitarity of V leads to conditions the matrix elements have to satisfy, e.g. $V_{ud}V_{ub}^* + V_{cd}V_{cb}^* + V_{td}V_{tb}^* = 0$. This condition can, in turn, be best visualized with the unitarity triangle, as shown in Fig. 1.

CP violation effects in B decays are potentially large due to the interference of amplitudes for the direct decay to a CP final state f_{CP} and the decay after mixing. This results in a decay rate asymmetry:

$$\begin{aligned} A_{CP}(t) &\equiv \frac{\Gamma(\bar{B}^0(t) \to f_{CP}) - \Gamma(B^0(t) \to f_{CP})}{\Gamma(\bar{B}^0(t) \to f_{CP}) + \Gamma(B^0(t) \to f_{CP})} \\ &= A_f \cos \Delta m_d t + S_f \sin \Delta m_d t. \end{aligned} \tag{1}$$

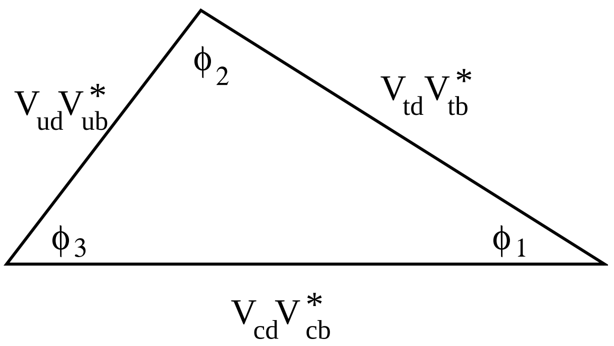

Figure 1: The unitarity triangle in the complex plane, corresponding to the condition $V_{ud}V_{ub}^* + V_{cd}V_{cb}^* + V_{td}V_{tb}^* = 0$.

Here Δm_d is the mass difference between the two B^0 mass eigenstates, and

$$A_f = \frac{|\lambda_f^2| - 1}{|\lambda_f^2| + 1}, S_f = \frac{2Im(\lambda_f)}{|\lambda_f^2| + 1}. \tag{2}$$

The complex parameter λ_f depends both on the amplitudes for the $B^0\bar{B}^0$ mixing and for the B^0 and $\bar{B}^0$ decay to f_{CP}. In the SM $|\lambda_f|$ equals to a good approximation to the absolute value of the ratio of the B^0 and $\bar{B}^0$ decay amplitudes.

The Standard Model predicts that for the decay channels involving $b \to c\bar{c}s$ transitions (e.g. $B \to J/\psi K_S$), A_f almost vanishes, and S_f amounts to $\sin 2\phi_1$. For the $b \to c\bar{c}d$ (e.g. $B \to J/\psi\pi^0$) decays, one again expects $A_f \approx 0$ and $S_f = \sin 2\phi_1$. Similarly, S_f should amount to $\sin 2\phi_1$, and A_f is predicted to be small in the $b \to s\bar{s}s$ (e.g. $B \to \phi K_S$) transitions. In the $b \to u\bar{u}d$ decays to final states like $\pi^+\pi^-$, A_f could differ sizeably from 0, and S_f could well deviate from the simple tree diagram prediction $\sin 2\phi_2$. We note that a deviation of A_f from 0 would indicate that $\Gamma(\bar{B} \to f_{CP}) \neq \Gamma(B \to f_{CP})$, which is a sign of direct CP violation.

1.1 Measurement of CP violation - principle

The branching fractions for $B \to f_{CP}$ decays are typically of order 10^{-4}. To carry out a CP violation experiment in the $B\bar{B}$ system, one therefore needs a large number of $B\bar{B}$ pairs (order of 100 million), which can best be produced and detected at a high luminosity asymmetric e^+e^- collider, a so called B-factory. There electrons and positrons with different energies collide to produce the $\Upsilon(4S)$ resonance, which then immediately decays into a coherent $B\bar{B}$ pair. When one of the B mesons decays into a flavour-specific final state, the flavour of the other B is tagged. If this B meson decays into a CP eigenstate f_{CP} at time Δt after flavour tagging,

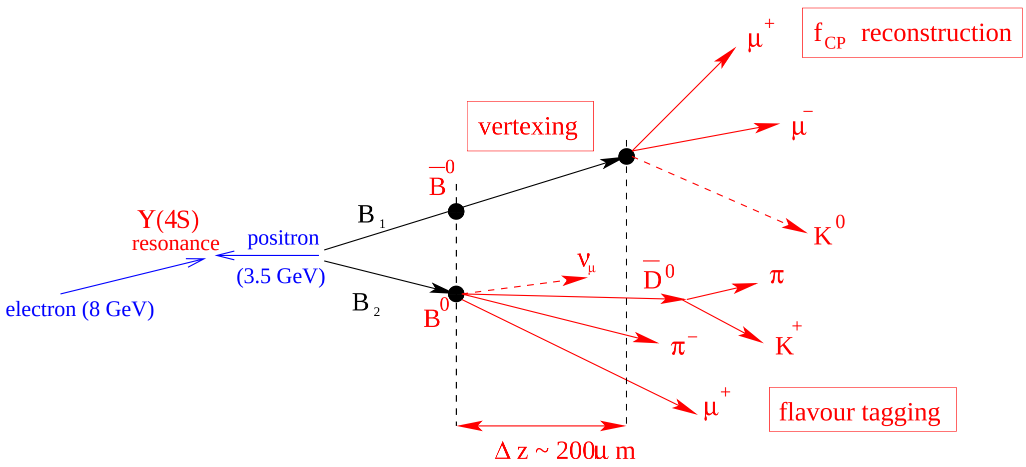

Figure 2: Principle of the CP violation measurement.

the asymmetry $A_{CP}(\Delta t)$ given in Eq. 1 can be measured. This measurement of the time difference Δt between the two decays is accomplished by measuring the distance between the decay vertices of the two mesons along the beam direction, $\Delta z = \beta\gamma c \Delta t$.

The decay products of the pair of B mesons (Fig. 2) are recorded in a spectrometer with precise vertexing, needed to determine the difference Δz. The spectrometer also has to provide accurate tracking in magnetic field to measure momenta of the decay products, as well as an efficient identification of electrons, muons, pions and kaons. In what follows the results of the measurements performed with the Belle spectrometer at the KEKB collider at KEK in Tsukuba in Japan will be presented.

1.2 Collider and spectrometer performance

In the KEKB symmetric collider [6], 8.0 GeV electrons collide with 3.5 GeV positrons at a small crossing angle ($\pm$11 mrad). The Lorentz boost factor of the center of mass system (cms) equals to $\beta\gamma = 0.425$. The peak luminosity of the KEKB collider is $7.4 \cdot 10^{33}$ cm^{-2}s^{-1}, and until July 2002 a data set corresponding to an integrated luminosity of 89.6 fb^{-1} was accumulated, out of which 78 fb^{-1} is on the $\Upsilon(4S)$ resonance, and the rest at a cms energy of 60 MeV below it.

The Belle spectrometer [7] performance is best summarized by the following figures of merit. The charged particle tracks are reconstructed in the Central Drift Chamber (CDC) with 50 layers of small drift cells. In the magnetic field of 1.5 T, the resolution in transverse momentum measurement is $\frac{\sigma_{p_T}}{p_T} \approx 0.35\%$ at 1 GeV/c. The reconstruction of tracks in the vicinity of the interaction point is performed by the Silicon Vertex Detector (SVD) with three double-sided silicon layers. The resulting accuracy in the impact parameter measurement is $\sigma = 55\ \mu$m for 1 GeV/c tracks perpendicular to the direction of the colliding beams.

For the identification of hadrons three systems are employed, a threshold Cherenkov counter with aerogel as radiator, a time of flight system and a measurement of the specific ionization dE/dx in the CDC. The resulting efficiency to identify a $K^{\pm}$ up to 3.5 GeV/c amounts to $\approx 90\%$, with a fake rate of $\approx 6\%$. Electrons are identified in the CsI electromagnetic calorimeter with a resolution of $\frac{\sigma_E}{E} \approx 1.8\%$ at 1 GeV. To identify muons and K_L mesons, an instrumented magnet yoke is used with 14 layers of resistive plate chamber (RPC) counters. The resulting identification efficiency for muons with momenta above 1 GeV/c exceeds 90% at a fake rate of 2%.

2 CP violation in the $b \to c\bar{c}s$ transitions

2.1 Reconstruction of CP eigenstates

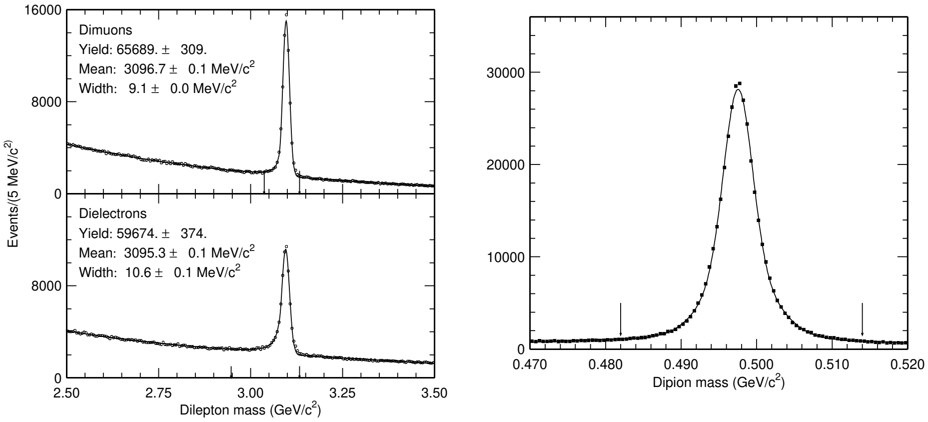

Figure 3: The invariant mass distribution of (a) $J/\psi \to \mu^+\mu^-, e^+e^-$ and (b $K_S \to \pi^+\pi^-$.

The decay channels of B^0 with CP eigenvalue $\xi_f = -1$, corresponding to $b \to c\bar{c}s$ transitions, were reconstructed in the charmonium-K_S final states as can be seen in Table 1. First the charmonium state was identified, two examples of which ($J/\psi \to \mu^+\mu^-, e^+e^-$) are shown in Fig. 3. The candidate was accepted after it passed a mode dependent cut on the invariant mass. Then the K_S was added, and for the combined state the beam constrained mass, $M_{\rm bc} = \sqrt{E^2_{\rm beam} - p^2_B}$, and the energy difference $\Delta E = E_B - E_{\rm beam}$, were used to identify the B meson decays. Here $E_{\rm beam}$ is the beam energy in the center of mass system, and E_B and p_B are the

$B^0 \to$	events	purity
$J/\psi K_S (K_S \to \pi^+\pi^-)$	1285	.976
$J/\psi K_S (K_S \to \pi^0\pi^0)$	188	.824
$\psi(2S) K_S$		
$(\psi(2S) \to \ell^+\ell^-) K_S$	91	.957
$(\psi(2S) \to J/\psi \pi^+\pi^-)$	112	.911
$\chi_{c1} K_S$	77	.958
$\eta_c (\eta_c \to K_S K \pi) K_S$	72	.646
$\eta_c (\eta_c \to K K \pi^0) K_S$	49	.725
$\eta_c (\eta_c \to p\bar{p}) K_S$	21	.936
$J/\psi K^* (K^* \to K_S \pi^0)$	101	.917
total $CP = -1$	1996	.935
$J/\psi K_L$, $CP = +1$	1330	.627
Total	3326	.807

Table 1: Reconstructed decay modes for full statistics corresponding to an integrated luminosity of 78 fb^{-1}, with the number of selected events and their purity.

cms energy and momentum of the reconstructed B candidate. The resulting $M_{\rm bc}$ distribution is shown in Fig. 4 where the signal events can be very clearly distinguished from the background. The corresponding purities are typically above 90% as can be seen in Table 1.

A different analysis had to be adopted in the reconstruction of the CP eigenvalue $\xi_f = +1$ final states, with a K_L and a J/ψ in the final state. Since K_L is detected in the ECL and KLM without any information on its energy, only its direction is known. The J/ψ candidate is combined with K_L direction, and the cms momentum $p_B^{\rm cms}$ of the resulting system is calculated assuming that it originates from the $B^0 \to J/\psi K_L$ decay. While the signal events should group around $p_B^{\rm cms} \approx 0.35$ GeV/c, the background should have a more uniform distribution. The shape of various backgrounds has been determined from MC simulation, and their sizes were deduced from a fit to the data as shown in Fig. 4. The fit yields 1330 signal events with a purity of 63%.

2.2 Measurement of Δt

The determination of Δt is accomplished by a measurement of the distance between the decay vertices of the tagging B and the B decay to the CP eigenstate f_{CP}, $\Delta z = \beta\gamma c \Delta t$. The resolution on the tagging B decay vertex is typically 140 μm (with a vertex reconstruction efficiency of $\epsilon = 91\%$), dominated by the products of subsequent charm decays. The resolution on the vertex of the f_{CP} decay amounts to 75 μm, and the efficiency is $\epsilon = 92\%$.

The accuracy of vertex determination is checked with a lifetime mea-

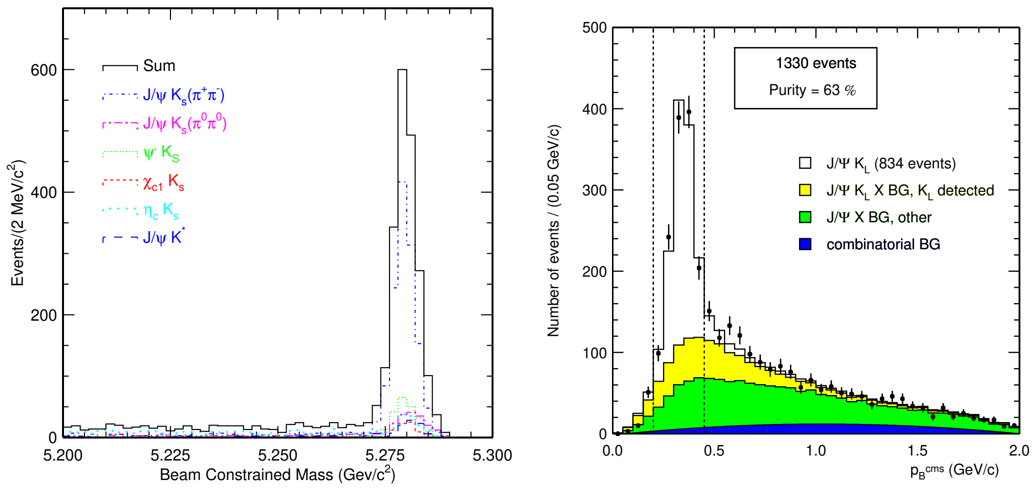

Figure 4: The beam energy constrained mass distribution for all event modes other than $J/\psi K_L$ (left), and the $p_B^{\rm cms}$ distribution for $B^0 \to J/\psi K_L$ candidates with results of the fit (right).

surement, for which the following decay modes[1] are used: $B^0 \to D^- \pi^+$, $D^{*-}\pi^+$, $D^{(*)-}\rho^+$, $B^0 \to J/\psi K_S$ and $B^0 \to J/\psi K^{*0}$. The typical time resolution is 1.43 ps, and the resulting estimate of the B^0 lifetime of 1.551 ± 0.018 (stat) ps [9] is in good agreement with the world average of 1.542 ± 0.016 ps [10].

2.3 Flavour tagging

To identify whether a B^0 or a $\bar{B}^0$ has decayed into the CP eigenstate, the decay products, charged leptons, kaons, pions, and Λ barions, of the associated tagging B are used. Events are classified by means of a discrete parameter q into those where the tagging B meson is more likely to be a B^0 ($q = +1$), and those where the tagging B meson is more likely to be a $\bar{B}^0$ ($q = -1$). Tagging is not perfect: there is always a chance w that the tag is fake (e.g. w is smaller for high momentum leptons, larger for tagging kaons). As a result, the asymmetry oscillation is reduced from $\sin \Delta m_d t$ to $(1-2w)\sin \Delta m_d t$, which is referred to as the raw asymmetry. Since the fit of the asymmetry is performed on an event-by-event basis, an estimate of the value of w is needed for each event. To accomplish this, events are classified into six categories in a tag quality variable r

[1] Throughout this paper, when a decay mode is quoted, the inclusion of the charge conjugate mode is implied.

according to the measured properties of the tracks used for tagging. The parameter r is determined by Monte Carlo, and ranges from $r = 0$ for no flavour discrimination to $r = 1$ for an unambigous flavour assignment. The relation between the correct tag probability $(1-2w)$ and parameter r is calibrated with data by using samples of exclusively reconstructed B^0 decays to self-tagging channels. The $B^0\bar{B}^0$ mixing oscillation, $(N_{of} - N_{sf})/(N_{of} + N_{sf}) = (1-2w)\cos\Delta m_d t$, with N_{of} and N_{sf} numbers of opposite and same flavour events, is used to determine the value of $(1-2w)$ for each interval in r as shown in Fig. 5.

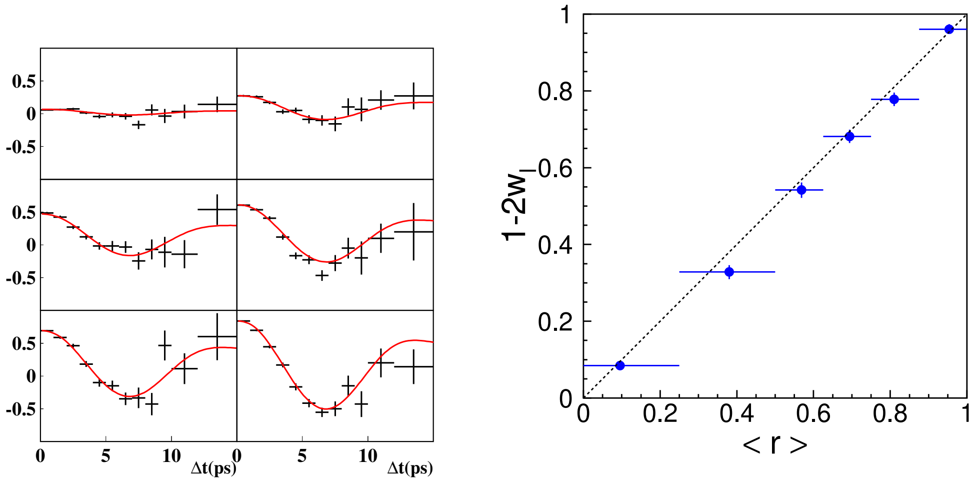

Figure 5: Calibration of flavour tagging algorithms: mixing oscillations in decays to self-tagging channels grouped in six intervals in r (left), and the resulting relation between the correct tag probability $(1-2w)$ and parameter r.

2.4 Results and cross-checks

Altogether 3326 events were reconstructed from a data sample corresponding to 78 fb^{-1}, out of which 2958 events had a valid vertex information, as well as a valid flavour tag. Out of these, in 1465 events the tagging particle is more likely to be a B^0 $(q = +1)$, while in 1493 events it is more likely to be a $\bar{B}^0$ $(q = -1)$. As can be seen from Fig. 6, the CP symmetry is clearly violated. The decays $\bar{B}^0 \to f_{CP=-1}$ (or $B^0 \to f_{CP=+1}$), depicted by open circles, differ from the decays $B^0 \to f_{CP=-1}$ (or $\bar{B}^0 \to f_{CP=+1}$), shown in full circles.

The value of $\sin 2\phi_1$ is determined from an unbinned maximum-likelihood fit to the observed Δt distributions. The probability density function

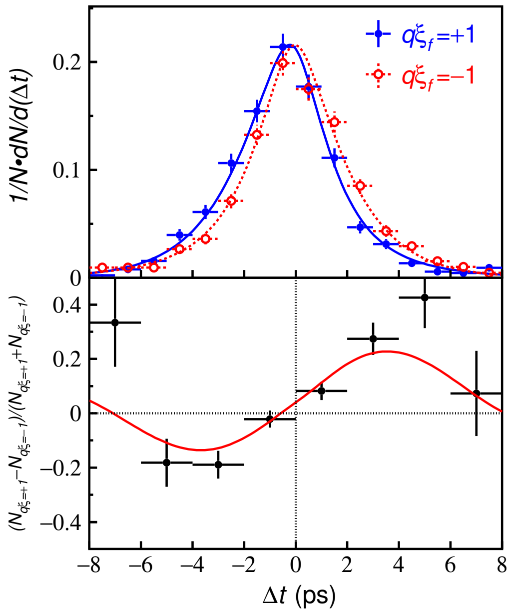

Figure 6: Top: Distributions over Δt for the events with $q\xi_f = +1$ (solid points) and $q\xi_f = -1$ (open points) in $b \to c\bar{c}s$ transitions. The results of the global fit with $\sin 2\phi_1 = 0.719$ are shown as solid and dashed curves, respectively. Bottom: the raw asymmetry for the same data set.

(PDF) expected for the signal distribution is given by

$$P_{sig}(\Delta t, q, w_l, \xi_f) = \frac{e^{-|\Delta t|/\tau_{B^0}}}{4\tau_{B^0}} \times [1 - q\xi_f(1-2w_l)\sin 2\phi_1 \sin(\Delta m_d \Delta t)], \quad (3)$$

with the B^0 lifetime τ_{B^0} and mass difference fixed to their world average values [10]. The PDF for combinatorial background events is modelled as a sum of exponential and prompt components convoluted with a sum of two Gaussians, the resolution function for the background. The only free parameter in the final fit is $\sin 2\phi_1$, which is determined by maximizing the likelihood function. The result of the fit is

$$\sin 2\phi_1 = 0.719 \pm 0.074 \pm 0.035 \quad (4)$$

The systematic uncertainties are dominated by vertexing (0.022) and the ambiguities in the resolution function (0.014), followed by a possible bias in the $\sin 2\phi_1$ fit (0.011) and $J/\psi K_L$ background fraction (0.010). The uncertainties in Δm_d and τ_B contribute each less than 0.010. In the fit we have assumed that $|\lambda_{ccs}| = 1$ (see Eq. 2), as it is indeed expected to be very close to unity in the SM. In order to test this assumption, we also performed a fit with $|\lambda_{ccs}|$ and S_{ccs} as free parameters. In this case we obtain $|\lambda_{ccs}| = 0.950 \pm 0.049 \pm 0.025$ and $-\xi_f S_f = 0.720 \pm 0.074$(stat) for all CP modes combined, where the sources of the systematic error for $|\lambda_{ccs}|$ are the same as those for $\sin 2\phi_1$. This result is consistent with the assumption used in our analysis.

To check for possible systematic effects, a comparison was made between the results as deduced from $CP = +1$ and $CP = -1$ decays. The two values, $\sin 2\phi_1 = 0.716 \pm 0.083$ for $CP = -1$, and $\sin 2\phi_1 = 0.78 \pm 0.17$ for $CP = +1$, agree very well. Another cross check was to carry out the same analysis for flavour specific final states, where there should be no asymmetry. The analyses of $B^0 \to D^{*\pm}\pi^{\mp}$ yielded "$\sin 2\phi_1$"$= 0.035 \pm 0.032$, $B^0 \to J/\psi K^{*0}$ (with $K^{*0} \to K^+\pi^-$) "$\sin 2\phi_1$"$= -0.021 \pm 0.093$, and $B^0 \to D^*\ell\nu$ "$\sin 2\phi_1$"$= 0.004 \pm 0.017$, all consistent with zero (see Fig. 7).

3 CP violation in $b \to u\bar{u}d$

As already discussed in Sec. 1, in the $b \to u\bar{u}d$ transitions such as the decay $B^0 \to \pi^+\pi^-$, the decay amplitude is a sum of a tree process (involving ϕ_2) and a penguin process (involving ϕ_1) [11]. As a result, $A_{\pi\pi} \neq 0$ and $S_{\pi\pi} \neq \sin 2\phi_2$ already in the SM. Moreover, in general $|\lambda_{\pi\pi}| \neq 1$, and $\Gamma(B^0 \to \pi^+\pi^-) \neq \Gamma(\bar{B}^0 \to \pi^+\pi^-)$, such that we can expect direct CP violation in this processes.

For the measurement presented here a data sample of 41.8 fb^{-1} was used [12]. Oppositely charged tracks, positively identified as pions, were used to construct candidate B mesons (see [13] for details). The background from $e^+e^- \to q\bar{q}$ continuum events was suppressed by using a

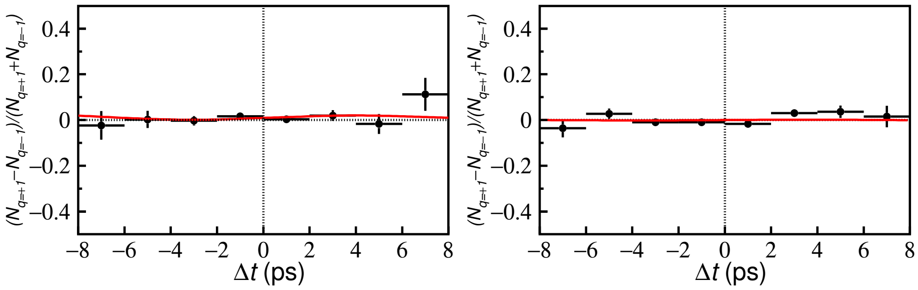

Figure 7: The raw asymmetry for the control channels $B^0 \to D^{*\pm}\pi^{\mp}$ and $B^0 \to D^*\ell\nu$.

Fisher discriminant [14] determined from six modified Fox-Wolfram moments [15], and the B meson direction in the cms with respect to the e^- beam axis. Again two variables in the cms frame, $M_{\rm bc}$ and ΔE, were used to discriminate the signal against the remaining backgrounds. After selecting events with $5.271\text{GeV}/c^2 < M_{\rm bc} < 5.287\text{GeV}/c^2$, we are left with a distribution shown in Fig. 8. A fit of intensities of individual background and signal components to the observed spectrum yields the following numbers of events in the signal region ($|\Delta E| < 0.067$ GeV): 73.5 ± 13.8 of the type $B^0 \to \pi^+\pi^-$, 28.4 ± 12.5 corresponding to the reaction $B^0 \to K^+\pi^-$, where K was misidentified as a π, and 98.7 ± 7.0 continuum events.

Flavour tagging and vertexing are done similarly as described for the $\sin 2\phi_1$ measurement. The Δt resolution function for the signal is a sum of two Gaussian functions, while for the continuum dominated background it is determined from the sideband region in $M_{\rm bc}$ and ΔE.

The CP violation parameters are determined with an unbinned maximum-likelihood fit to the observed Δt distribution (Fig. 9). The corresponding PDF takes into account the purity of the events as a function of $M_{\rm bc}$ and ΔE. The result is

$$S_{\pi\pi} = -1.21^{+0.38}_{-0.27}{}^{+0.16}_{-0.13},$$

$$A_{\pi\pi} = +0.94^{+0.25}_{-0.31} \pm 0.09.$$

The systematic error on $S_{\pi\pi}$ is dominated by the uncertainties in background fractions (± 0.09) and a possible fit bias close to the physical boundary ${}^{+0.11}_{-0.02}$. The main contributions to the systematic error on $A_{\pi\pi}$ come from the uncertainties in background fractions (± 0.06) and wrong-tag fractions (± 0.06).

As one of the cross-checks, the reaction $B^0 \to K\pi$ was analyzed in the same way. As expected, in this case no asymmetry could be observed in the Δt distribution, $S_{K\pi} = 0.15 \pm 0.24$, and $A_{K\pi} = 0.07 \pm 0.17$. As an additional test of the background treatment, we perform the fit on the events from the $B^0 \to \pi\pi$ sidebands, and get $S = 0.08 \pm 0.06$, $A = 0.03 \pm 0.04$, again consistent with a null asymmetry.

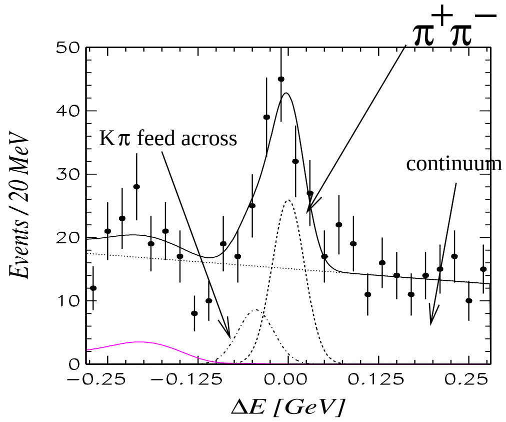

Figure 8: The ΔE distribution of the $B^0 \to \pi^+\pi^-$ decay candidates. The result of the fit to data is shown as a solid curve, and the contributions from the signal and different background sources are depicted by dashed, dotted and dash-dotted curves.

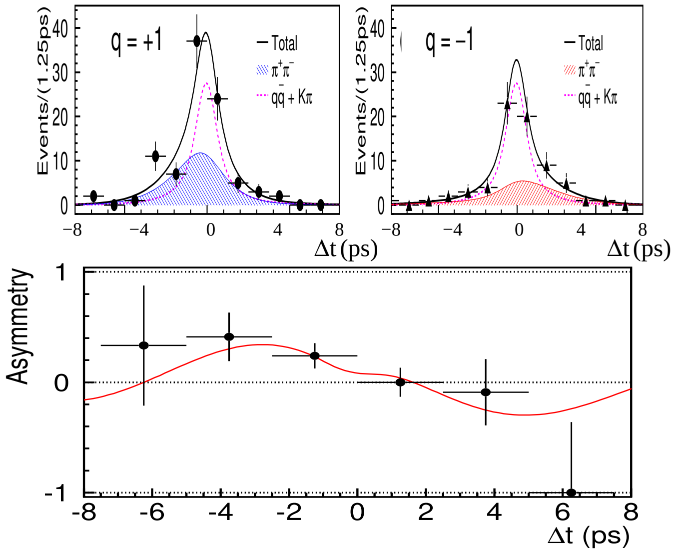

Figure 9: The Δt distributions for the two classes of event, with $q = +1$ and $q = -1$ (top), and the raw asymmetry (bottom). In the top two pictures the contributions of individual components, $\pi\pi$ and background from $q\bar{q}$ and $K\pi$ are indicated.

4 CP violation in $b \to s\bar{s}s$

In the Standard Model, the time evolution coefficients for the process $b \to s\bar{s}s$, of which $B^0 \to \eta' K$ is an example, are the same as for $b \to c\bar{c}s$, $S_{sss} = -\xi_f \sin 2\phi_1$, $A_{sss} \approx 0$, where again ξ_f is the CP eigenvalue of f_{CP}. This transition is interesting since a significant deviation from the SM prediction is allowed, if there is an additional CP-violating phase other than that in the KM scheme [16].

In the present analysis the full data sample, corresponding to the integrated luminosity of 78 fb^{-1}, was used to measure for the first time CP violation in the $B^0 \to \phi K_S$ and $K^+K^-K_S$ channels, and to improve the measurement in the decay $B^0 \to \eta' K_S$ [17]. In the channel $B^0 \to \eta' K_S$, the following decay chains were considered: $\eta' \to \pi^+\pi^-\eta$ (with $\eta \to \gamma\gamma$) and $\eta' \to \rho\gamma$ (with $\rho \to \pi^+\pi^-$). From the measured distribution of $M_{\rm bc}$ for the candidate events, shown in Fig. 10, $N(B^0 \to \eta' K_S) = 147.9 \pm 14.6$ is extracted. For $B^0 \to \phi K_S$, reconstructed in the $\phi \to K^+K^-$, $K_S \to \pi^+\pi^-$ final state, $N(B^0 \to \phi K_S) = 35.4 \pm 2.9$ is deduced [18]. In the channel $B^0 \to K^+K^-K_S$ with $K_S \to \pi^+\pi^-$, the K^+K^- is required not to come from a ϕ decay, and $N(B^0 \to K^+K^-K_S) = 94.3 \pm 7.3$ is found, all in a data sample corresponding to the integrated luminosity of 78 fb^{-1}. The $B^0 \to K^+K^-K_S$ decay is found to be primarily a transition to a $\xi_f = +1$ state, with the $\xi_f = -1$ contribution of $0.03 \pm 0.15(\text{stat}) \pm 0.07(\text{syst})$ [19].

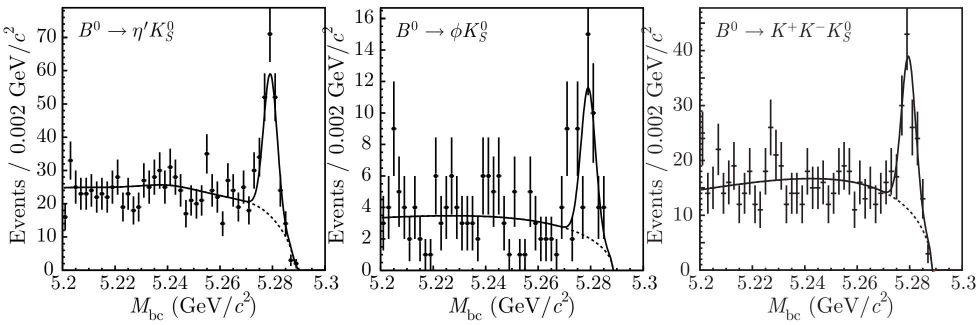

Figure 10: Distribution of the beam constrained mass for the channels $B^0 \to \eta' K_S$ (left), $B^0 \to \phi K_S$ (middle) and $B^0 \to K^+K^-K_S$ (right).

The raw asymmetries, corresponding to the three channels, are shown in Fig. 11. The following time evolution coefficients are found from a fit to the corresponding Δt distributions, $-\xi_{\eta' K} S_{\eta' K} = 0.71 \pm 0.37^{+0.05}_{-0.06}$, $A_{\eta' K} = +0.26 \pm 0.22 \pm 0.03$, $-\xi_{\phi K} S_{\phi K} = -0.73 \pm 0.64 \pm 0.18$, $A_{\phi K} = -0.56 \pm 0.41 \pm 0.12$, and $-\xi_{KKK} S_{KKK} = 0.52 \pm 0.46 \pm 0.11^{+0.27}_{-0.03}$, $A_{KKK} = -0.43 \pm 0.36 \pm 0.10^{+0.03}_{-0.22}$. The KKK channel has an additional systematic error contribution coming from the uncertainty in the $CP = \pm 1$ fractions, $w = (3^{+16}_{-3})\%$. The values obtained for $-\xi_f S_f$ are consistent with the

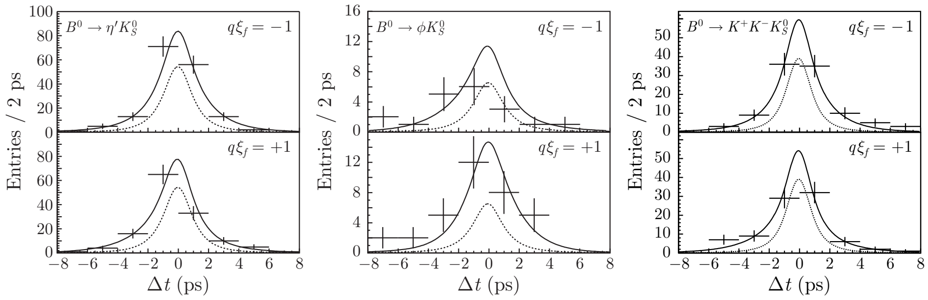

Figure 11: The Δt distribution for the channels $B^0 \to \eta' K_S$ (left), $B^0 \to \phi K_S$ (middle) and $B^0 \to K^+K^-K_S$ (right), shown separatelly for $q\xi_f = -1$ (top) and $q\xi_f = -1$ (bottom) candidates. The solid curves show the results of the global fits, and the dashed ones the background distributions.

world average of $\sin 2\phi_1 = 0.734 \pm 0.054$ [20] in the $B^0 \to K^+K^-K_S$ and $B^0 \to \eta' K_S$ decays, while a 2.2σ deviation is observed in $B^0 \to \phi K_S$.

The main systematic errors are due to uncertainties in resolution function parameters ($^{+0.03}_{-0.04}$ for S_f) and the signal fraction (± 0.02 for A_f) for the $B^0 \to \eta' K_S$ decay, vertex reconstruction (± 0.09 for S_f and ± 0.08 for A_f) for $B^0 \to K^+K^-K_S$, while for $B^0 \to \phi K_S$ the primary source is the uncertainty in the signal fraction and the background shape in Δt (in total ± 0.16 for S_f and ± 0.12 for A_f).

5 CP violation in $b \to c\bar{c}d$

The parameters of CP violation were also determined for the first time in one of the $b \to c\bar{c}d$ transitions, the decay channel $B^0 \to J/\psi\pi^0$, a $CP = +1$ eigenstate. The data sample considered again corresponded to the 78 fb^{-1} of integrated luminosity. From the $M_{\rm bc}$ distribution of candidate events, shown in Fig. 12, 49.1 ± 1.3 events were attributed to the signal channel [21]. A fit to the corresponding Δt distribution (Fig. 12) yielded $-S_{J/\psi\pi} = +0.93 \pm 0.49 \pm 0.08$ and $A_{J/\psi\pi} = -0.25 \pm 0.39 \pm 0.06$. Both values are within error in agreement with the SM expectation, $-S_{J/\psi\pi} = \sin 2\phi_1$ and $A_{J/\psi\pi} = 0$.

6 Measurement of $B \to X_s \ell^+ \ell^-$

In the SM, the lowest order diagrams for the flavour-changing neutral current process $b \to s\ell\ell$ are loop (penguin) and box diagrams of a virtual top quark and a weak boson. Non-SM contributions [22] could either enter as tree diagrams or as non-SM particles loop and box diagrams, and could modify sizeably the SM decay amplitude, for which the next-to-next-to-leading order (NNLO) corrections have been calculated [23]. The

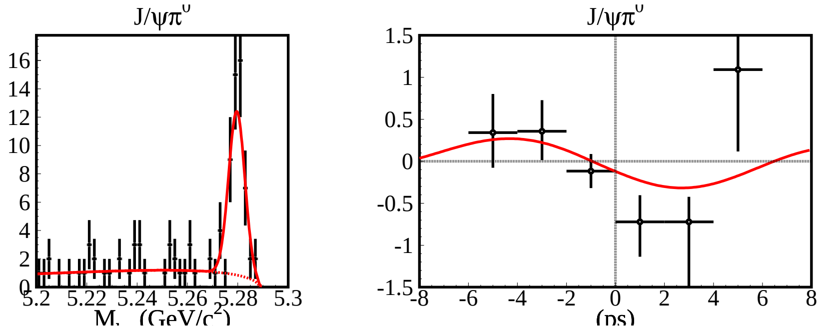

Figure 12: Distribution of the beam constrained mass (left) and raw asymmetry (rigt) for the channel $B^0 \to J/\psi\pi^0$ (left).

first observation of such decay type, $B \to K\ell^+\ell^-$, by Belle [24] recently opened this new window in the search for physics beyond the SM. Here we present results of a measurement of the branching fraction for the inclusive decay $B \to X_s\ell^+\ell^-$ on a data sample corresponding to an integrated luminosity of 60 fb^{-1} [25]. B is either B^0 or B^+, ℓ is either and electron or a muon, and X_s is a hadronic recoil system that contains a kaon. The hadronic system is reconstructed from a charged kaon or K_S combined with 0 to 4 pions, of which up to one π^0 is allowed. These combinations cover $(81 \pm 2)\%$ of the total inclusive decays. The combination of X_s with two oppositely charged leptons is identified as a $B \to X_s\ell^+\ell^-$ signal by making use of the beam energy constrained mass, $M_{\rm bc}$, and the energy difference, ΔE.

The largest background source are random combinations of dileptons with a kaon and pions, from continuum $q\bar{q}$ ($q = u, d, s, c$) production or from semileptonic B decays. These two backgrounds do not produce signal-like peaks in $M_{\rm bc}$ and ΔE. The $q\bar{q}$ background is again suppressed by using a Fisher discriminant based on a modified set of Fox-Wolfram moments [15]. Events with $M_{\ell\ell} < 0.2$ GeV$/c^2$ are rejected in order to suppress electron pairs from π^0 Dalitz pair decays and γ conversions. The semileptonic B decay background, where either B mesons decay into leptons or two leptons are produced in the $b \to c \to s, d$ decay chain, are suppressed by rejecting events with two neutrinos with a cut on another Fisher discriminant, based on total visible energy of the event and the missing mass.

For events with multiple candidates that pass the selection criteria, we choose the combination with the largest signal probability, which is estimated by ΔE and the B flight direction with respect to the e^- beam direction in cms. We then reject candidates with hadronic recoil mass M_{X_s} greater than 2.1 GeV$/c^2$. This condition removes a significant fraction of the combinatorial background while retaining $(93 \pm 5)\%$ of the signal.

Two remaining backgrounds are removed in the following way. The

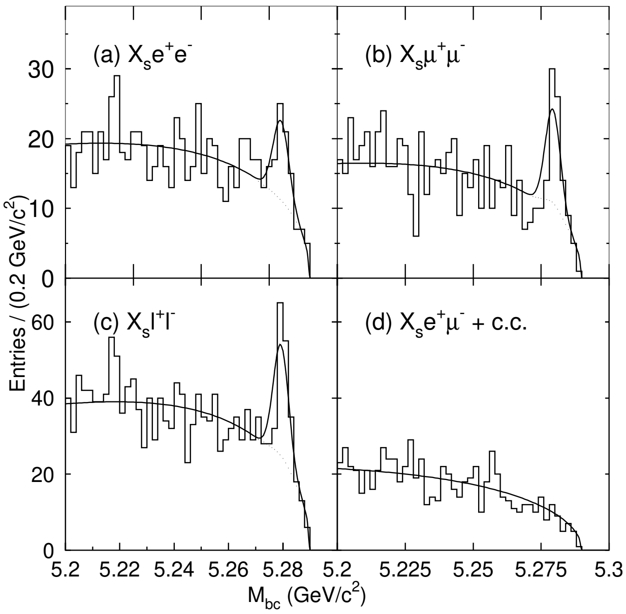

Figure 13: $M_{\rm bc}$ distribution of candidate events $B \to X_s\ell^+\ell^-$.

background from $B \to X_s J/\psi(\to \ell^+\ell^-)$ and $X_s\psi(2S)(\to \ell^+\ell^-)$ decays is removed by cutting out the two corresponding regions in the $M_{\ell\ell}$ invariant mass. The contamination from $B \to X_s\pi^+\pi^-$ due to pion misidentification is removed by subtracting the corresponding expected contributions (4.5 events for $\mu\mu$, 0.2 for ee), as determined from MC simulation.

We determine the reconstruction efficiency with MC samples, where we model the signal characteristics as follows. The NNLO calculations of Ref. [26] are used for the $M_{\ell\ell}$ spectrum. The hadronic recoil mass M_{X_s} spectrum is modelled by a sum of the exclusive $B \to K\ell^+\ell^-, K^*\ell^+\ell^-$ components and an inclusive component based on a Fermi motion model [27] above 1.1 GeV/c^2. The hadronisation of the quark systems ($s\bar{d}$ and $s\bar{u}$) is treated with the JETSET program [28]. The requirement $M_{\ell\ell} > 0.2$ GeV/c^2 removes the virtual photon contribution, $b \to s\gamma^* \to se^+e^-$, and makes the predicted rates for the two modes approximately equal: $Br(B \to X_s e^+e^-) \sim Br(B \to X_s\mu^+\mu^-) \sim (4.2 \pm 0.7) \times 10^{-6}$ [29]. Based on this assumption we take the average of the two to obtain the $B \to X_s\ell^+\ell^-$ branching fraction. The expected $M_{\ell\ell}$ and M_{X_s} spectra are shown in Figs. 14(a) and (b), respectively. The resulting reconstruction efficiencies are $(3.9 \pm 0.4 \pm 0.5)\%$ for $B \to X_s e^+e^-$ and $(3.6 \pm 0.4 \pm 0.5)\%$ for $B \to X_s\mu^+\mu^-$, where the first error is systematic and the second is due to the model uncertainties, mainly in the fractions of the exclusive components (11%). The systematic error comes from K_S and π^0 reconstruction efficiency (8.7% per K_S, 6.8% per π^0), electron identification (1.8% per electron), muon identification (2.2% per muon), K^+ identification (2.5% per K^+), π^+ identification (0.8% per π^+), and the background suppression criteria (3.0%).

The signal yield is determined from an unbinned maximum likelihood fit to the $M_{\rm bc}$ distribution, as shown in Fig. 13. We model the signal with a Gaussian function and the background with a threshold function [30]. The resulting branching fraction is

$$BR(B \to X_s\ell^+\ell^-) = (6.1 \pm 1.4^{+1.3}_{-1.1}) \cdot 10^{-6}$$

for $M_{\ell\ell} > 0.2$ GeV/c^2. The systematic errors in the yield, efficiency, the number of B meson pairs and the model errors are added in quadrature to give the total systematic error.

The dilepton mass and recoil mass spectra are measured by dividing the data into $M_{\ell\ell}$ and M_{X_s} bins. For each bin, the signal yield is again extracted from a fit to the $M_{\rm bc}$ distribution and the fake background contribution is subtracted. The results are shown in Fig. 14(c) and (d). In the recoil mass M_{X_s} spectrum the $B \to K\ell^+\ell^-$ signal is clearly seen, $B \to K^*\ell^+\ell^-$ is not significant, and we have additional contributions for $M_{X_s} > M_{K^*}$. With the current statistics, the $M_{\ell\ell}$ and M_{X_s} spectra are in agreement with the SM expectations. Note that the number of observed events in the K region is consistent with the exclusive measurement [24].

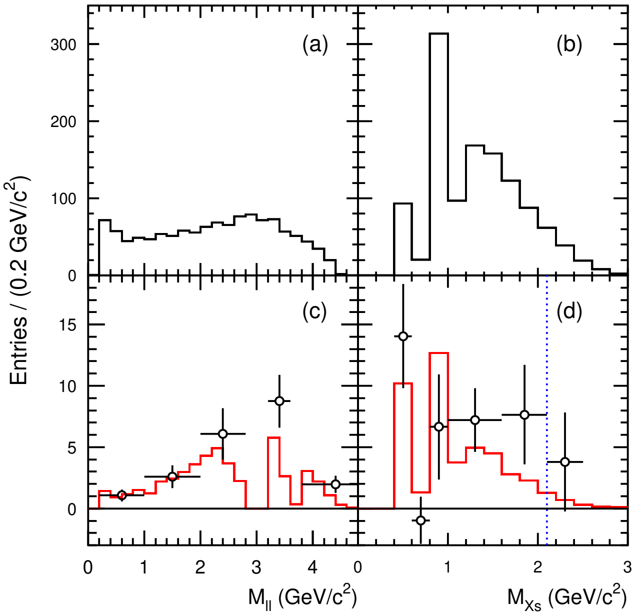

Figure 14: SM expectations for the (a) dilepton and (b) recoil mass spectra; the observed (c) dilepton and (d) recoil mass spectra (circles). The histograms in (c) and (d) show the SM expectations after all the selection criteria are applied; histograms are normalized to the expected branching fractions. The dotted line in (d) indicates the $M_{X_s} < 2.1$ GeV/c^2 requirement for the branching fraction measurement.

7 Summary

We have measured the CP violation parameters in B^0 decays to the following CP eigenstates: $(c\bar{c})K_S$, $J/\psi K_L$, $J/\psi K^{*0}$, $\pi^+\pi^-$, ϕK_S, $\eta' K_S$, $K^+K^-K_S$ and $J/\psi\pi^0$, using data collected at the $\Upsilon(4S)$ resonance with the Belle detector at the KEKB asymmetric e^+e^- collider.

One of the angles of the unitarity triangle, ϕ_1, has been determined using 78 fb^{-1} as:

$$\sin 2\phi_1 = 0.719 \pm 0.074 \pm 0.035. \tag{5}$$

The large $A_{\pi\pi}$ found in the $B^0 \to \pi^+\pi^-$ decay is an indication of direct CP violation in B meson decay, and suggests that there is a large hadronic phase and interference between the tree and penguin amplitudes. In this case the precise determination of $\sin 2\phi_2$ from $S_{\pi\pi}$ requires additional measurements including the branching fractions for the decays $B^0 \to \pi^0\pi^0$ [32].

The decays, $B^0 \to \phi K_S$, $\eta' K_S$ and $K^+K^-K_S$ are dominated by the $b \to s\bar{s}s$ transition and are sensitive to a new CP-violating phase. Our results are consistent with those obtained for the $B^0 \to J/\psi K_S$ and other decays governed by the $b \to c\bar{c}s$ transition within 3σ. The larger data sample recorded at Belle will allow for further study with higher precision in the near future.

We also present the first measurement of the inclusive branching fraction for the electroweak penguin decay $B \to X_s\ell^+\ell^-$. The results on the branching fraction, dilepton and recoil mass spectra are in agreement with the SM expectations and can be used to constrain extensions of the SM.

Acknowledgments

We would like to thank the organizers of this well organized conference for inviting us to present our results. We also would like to acknowledge the KEKB accelerator group for the excellent operation of the machine.

References

[1] H. Albrecht *et al.* (ARGUS Collaboration), Phys. Lett. **B192**, 245 (1987).

[2] A. B. Carter and A. I. Sanda, Phys. Rev. D **23**, 1567 (1981); I. I. Bigi and A. I. Sanda, Nucl. Phys. **B193**, 85 (1981).

[3] Belle Collaboration, K. Abe *et al.*, Phys. Rev. Lett. **87**, 091802 (2001); Belle Collaboration, K. Abe *et al.*, hep-ex/0202027 (to be published).

[4] BaBar Collaboration, B. Aubert *et al.*, Phys. Rev. Lett. **87**, 091801 (2001); BaBar Collaboration, B. Aubert *et al.*, hep-ex/0201020, submitted to Phys. Rev. D.

[5] M. Kobayashi and T. Maskawa, Prog. Theor. Phys. **49**, 652 (1973).

[6] KEK Report No. 2001-157, edited by E. Kikutani, 2001, to be published in Nucl. Instrum. Methods Phys. Res. A.

[7] Belle Collaboration, A. Abashian *et al.*, Nucl. Instrum. Methods Phys. Res. A **479**, 117 (2002).

[8] Belle Collaboration, K. Abe *et al.*, Phys. Lett. B **538**, 11 (2002).

[9] Belle Collaboration, K. Abe *et al.*, Phys. Rev. Lett. **88**, 171801 (2002).

[10] Particle Data Group, K. Hagiwara *et al.*, Phys. Rev. D **66**, 010001 (2002).

[11] M. Gronau, Phys. Rev. Lett. **63**, 1451 (1989); D. London and R. Peccei, Phys. Lett. B **223**, 257 (1989); M. Beneke, G. Buchalla, M. Neubert and C. T. Sachrajda, Nucl. Phys. B **606**, 245 (2001); Y. Y. Keum, H-N. Li and A. I. Sanda, Phys. Rev. D **63**, 054008 (2001); M. Ciuchini *et al.*, Phys. Lett. B **515**, 33 (2001); M. Gronau and J. L. Rosner, Phys. Rev. D **65**, 013004 (2002).

[12] Belle Collaboration, K. Abe *et al.*, Phys. Rev. Lett. **89**, 071801 (2002).

[13] K. Abe *et al.* (Belle Collab.), Phys. Rev. Lett. **87**, 101801 (2001); a Phys. Rev. D paper is in preparation.

[14] R. A. Fisher, Annals Eugen. **7**, 179 (1936).

[15] The Fox-Wolfram moments were introduced in G. C. Fox and S. Wolfram, Phys. Rev. Lett. **41**, 1581 (1978). The Fisher discriminant used by Belle is described in [13] and K. Abe *et al.* (Belle Collab.), Phys. Lett. **B 511**, 151 (2001).

[16] Y. Grossman and M. P. Worah, Phys. Lett. B **395**, 241 (1997); T. Moroi, Phys. Lett. B **493**, 366 (2000); D. Chang, A. Masiero and H. Murayama, hep-ph/0205111 (2002).

[17] K.-F. Chen and K. Hara *et al.*, hep-ex/0207033 (2002).

[18] Belle Collaboration, A. Bozek *et al.*, unpublished.

[19] Belle Collaboration, A. Garmash *et al.*, BELLE-CONF-0225 (2002).

[20] Y. Nir, hep-ph/0208080 (2002).

[21] Belle Collaboration, K. Abe *et al.*, BELLE-CONF-0209 (2002).

[22] For example, E. Lunghi, A. Masiero, I. Scimemi and L. Silverstrini, Nucl. Phys. **B568**, 120 (2000); J. L. Hewett and J. D. Wells, Phys. Rev. **D55**, 5549 (1997); T. Goto, Y. Okada, Y. Shimizu and M. Tanaka, Phys. Rev. **D55**, 4273 (1997); G. Burdman, Phys. Rev. **D52**, 6400 (1995); N. G. Deshpande, K. Panose and J. Trampetić, Phys. Lett. **B308**, 322 (1993); W. S. Hou, R. S. Willey and A. Soni, Phys. Rev. Lett. **58**, 1608 (1987).

[23] C. Bobeth, M. Misiak and J. Urban, Nucl. Phys. **B574**, 291 (2000); H. H. Asatrian, H. M. Asatrian, C. Greub and M. Walker, Phys. Lett. **B507**, 162 (2001).

[24] K. Abe *et al.* (Belle Collaboration), Phys. Rev. Lett. **88**, 021801 (2002).

[25] Belle Collaboration, J. Kaneko *et al.*, hep-ex/0208029, submitted for publication in Phys. Rev. Lett.

[26] A. Ali, E. Lunghi, C. Greub and G. Hiller, hep-ph/0112300; A. Ali, P. Ball, L. T. Handoko and G. Hiller, Phys. Rev. **D61**, 074024 (2000).

[27] A. Ali, G. Hiller, L. T. Handoko and T. Morozumi, Phys. Rev. **D55**, 4105 (1997).

[28] T. Sjöstrand, "PYTHIA 5.6 and JETSET 7.3: Physics and manual", CERN-TH-6488-92.

[29] Calculated by the original authors based on Ref. [26].

[30] H. Albrecht *et al.* (ARGUS Collaboration), Phys. Lett. **B229**, 304 (1989).

[31] $S_{\pi\pi} = 0.03^{+0.53}_{-0.56}(\text{stat}) \pm 0.11(\text{syst})$ and $C_{\pi\pi} = -0.25^{+0.45}_{-0.47}(\text{stat}) \pm 0.14(\text{syst})$ in B. Aubert *et al.* (BaBar Collab.), Phys. Rev. D **65**, 051502R (2002). Note that the sign convention for the coefficient of the cosine term $C_{\pi\pi}$ defined in the above reference is in the opposite of our convention, i.e. $C_{\pi\pi} = -A_{\pi\pi}$.

[32] M. Gronau and D. London, Phys. Rev. Lett. **65**, 3381 (1990); M. Gronau, D. London, N. Sinha and R. Sinha, Phys. Lett. B **514**, 315 (2001).